The role of three-dimensional fault interactions in creating complex seismic sequences and power-law magnitude distributions

Yifan Yin[1], Percy Galvez[2], Elias Rafn Heimisson[3], and Stefan Wiemer[3]

[1]Swiss Seismological Service
[2]King Abdullah University of Science and Technology
[3]ETH Zurich

February 27, 2023

Abstract

A physics-based earthquake simulator should reproduce first-order empirical power-law behaviors of magnitudes and clustering. However, sequences exhibiting these laws have only been produced in discrete and low-dimension continuum simulations. We show that the same emergence also occurs in 3-D continuum simulations. Our model approximates a strike-slip fault system slipping under rate-and-state friction. We produce spatiotemporally clustered earthquake sequences exhibiting characteristic Gutenberg-Richter scaling as well as empirical inter-event time distribution. With fault interaction, partial ruptures emerge when seismogenic width W over characteristic nucleation length $L_{[?]}$ is larger than 16.24, but none occurs without fault interaction. The mainshock recurrence times of individual faults remain quasi-periodic and fit a Brownian passage time distribution. The system mainshock recurrence time has a short-term Omori-type decay, indicating a 22% chance of mainshock clustering. These results show that physics-based multi-cycle models adequately reflect observed statistical signatures and show practical potential for long-term hazard assessment and medium-term forecasting.

Hosted file

`essoar.10510908.1.docx` available at https://authorea.com/users/524278/articles/595433-the-role-of-three-dimensional-fault-interactions-in-creating-complex-seismic-sequences-and-power-law-magnitude-distributions

Hosted file

`yinyifan.grl.manuscript.suppl.docx` available at https://authorea.com/users/524278/articles/595433-the-role-of-three-dimensional-fault-interactions-in-creating-complex-seismic-sequences-and-power-law-magnitude-distributions

The role of three-dimensional fault interactions in creating complex seismic sequences and power-law magnitude distributions

Y. Yin[1], P Galvez[2], E. R. Heimisson[1] and S. Wiemer[1]

[1] Swiss Seismological Service, ETH Zurich, Zurich, Switzerland

[2] King Abdullah University of Science and Technology (KAUST), Thuwal, Saudi Arabia

Corresponding author: Yifan Yin (yifan.yin@sed.ethz.ch)

Key Points:

- We model three en echelon strike-slip faults governed by rate-and-state friction using a quasi-dynamic approach and an improved solver.

- The simulations produce power-law distributed earthquake sequences both in size and inter-event times in a well-resolved 3-D continuum.

- The recurrence time distribution shows a 22% chance of mainshock clustering within the fault system.

Abstract

A physics-based earthquake simulator should reproduce first-order empirical power-law behaviors of magnitudes and clustering. However, sequences exhibiting these laws have only been produced in discrete and low-dimension continuum simulations. We show that the same emergence also occurs in 3-D continuum simulations. Our model approximates a strike-slip fault system slipping under rate-and-state friction. We produce spatiotemporally clustered earthquake sequences exhibiting characteristic Gutenberg-Richter scaling as well as empirical inter-event time distribution. With fault interaction, partial ruptures emerge when seismogenic width W over characteristic nucleation length L_∞ is larger than 16.24, but none occurs without fault interaction. The mainshock recurrence times of individual faults remain quasi-periodic and fit a Brownian passage time distribution. The system mainshock recurrence time has a short-term Omori-type decay, indicating a 22% chance of mainshock clustering. These results show that physics-based multi-cycle models adequately reflect observed statistical signatures and show practical potential for long-term hazard assessment and medium-term forecasting.

Plain Language Summary

Earthquakes famously exhibit power-law statistics regarding event size and the time between events. This means, for example, that for every magnitude 6, there are about 10 magnitude 5 events. To date, it has been challenging to simulate earthquakes on a computer that produces these statistics and at the same time have a resolved rupture in 3-D, meaning that the space-time evolution of each earthquake rupture is simulated in realistic detail. Our research shows that a

3-D simulation of multiple faults can naturally produce these observed statistics. We simulate a system of three strike-slip faults in echelon formation in an elastic medium. The simulations produce full ruptures and partial ruptures when the width of the seismogenic zone is significantly greater than a characteristic length scale. We investigate the likelihood of the next event happening, either on the same fault or on any fault within the system. We find that whenever a mainshock occurs, there is a one-fifth chance that the next mainshock will follow soon in the model. Our result shows that these models have the potential to give a better estimate of seismic hazard of a 100-year horizon.

Index Terms and Keywords

0545 Modeling

7223 Earthquake interaction, forecasting, and prediction

8111 Continental tectonics: strike-slip and transform

Earthquake cycle; rate-and-state friction; fault system; recurrence time

1 Introduction

Empirical seismicity, earthquake rupture, and fault observations are inherently multi-scale in space and time (Ben-Zion, 2008; Faulkner et al., 2010). Existing numerical models of earthquake processes adopt either a discrete approach to reproducing the statistical properties of regional seismicity or a continuum approach that simulates the complexities of single-event rupture processes (Erickson et al., 2020; Tullis et al., 2012). A large gap remains between the two approaches. Narrowing this gap would be desirable to build more realistic earthquake simulators, which are crucial for enhancing process understanding and probabilistic seismic hazard assessment (PSHA).

When considered as point processes, earthquakes are discrete in time with well-known empirical distributions. The earthquake size distribution follows the Gutenberg-Richter power law (Gutenberg & Richter, 1944), aftershock and foreshock statistics follow the Omori-Utsu law (Omori, 1895; Utsu, 1961), and inter-event time can be described using the Omori-Utsu law plus Poisson process (Saichev & Sornette, 2007). Statistical models such as Epidemic-Type Aftershock Sequence (ETAS) are based on these empirically observed laws (Ogata, 1988). ETAS can reproduce and forecast the seismicity surprisingly well, outperforming physics-based models in retrospective and prospective experiments, especially for aftershock forecasts (Ogata, 1988; Schorlemmer et al., 2018). While ETAS-type models are shown to be successful for operational earthquake forecasts for short horizons (Taroni et al., 2018), a long-term assessment still requires fault-based seismicity evaluated based on observations (e.g., geodesy, historical earthquake catalogs, paleoseismology) combined with first-order physical concepts like elastic rebound as the basis (Field et al., 2017).

A popular way to describe discrete complex systems such as seismicity is based on cellular automata models. These models use simplified rules of interaction

as an analogy to stress transfer to produce similar statistics (Bak & Tang, 1989; Huang & Turcotte, 1990; Jiménez, 2013). The somewhat arbitrarily defined rules fail to represent a wide range of physical observations and processes, such as slow-slip events and non-volcanic tremors that affect earthquake productivity (Beroza & Ide, 2011). Newer earthquake simulators attempt to represent earthquake interactions more realistically by creating cellular automata models using realistic fault geometries, realistic strain-stress relationships, and a failure criterion (Tullis et al., 2012). The RSQSim simulator is particularly successful in that it incorporates a simplified version of rate-and-state friction (RSF) to create sequences that satisfy scaling laws and foreshock and aftershock clustering (Dieterich & Richards-Dinger, 2010; Richards-Dinger & Dieterich, 2012). However, the simulator is still inherently discrete and thus suffers from the grid dependence of such models (Rice, 1993). This means that if one changes the grid size or meshing method, the resulting sequences and behavior will also change. The RSQSim simulator mitigates the influence of grid dependence on rupture propagation by altering the friction law in an ad-hoc manner (Richards-Dinger & Dieterich, 2012).

Researchers use inherently discrete models for synthetic seismicity because using a well-resolved 3-D continuum model is computationally expensive. A simulation is well resolved if the smallest physical length scale is resolved by several patches that evolve together as a continuum. This critical size generally considered to be the cohesive zone size of an unstable slip (equation 4) (Lapusta et al., 2000; Rubin & Ampuero, 2005). This continuum limit requires the mesh to be much finer than discrete earthquake simulators, whose patches are allowed to fail individually. More importantly, a simulation that satisfies the continuum limit does not necessarily produce power-law distributed seismicity but only characteristic or simple cycling events. Thus, to create catalogs with certain distributions, studies impose distributions of critical slip distance on the fault surface (Galvez et al., 2019; Hillers et al., 2007) and hence condition the simulation to reproduce the desired behavior.

Despite the computational barrier, physics-based models are vital to advancing our understanding of the rupture process and improving forecasts, whether by testing friction laws, testing fault properties, or combining other physical processes in both industrial and tectonic settings (Dublanchet, 2020; van den Ende et al., 2018; Larochelle et al., 2021; Noda & Lapusta, 2013; Weng & Ampuero, 2019). Forecasts can be greatly improved by assimilating past sequences and real-time data into models (van Dinther et al., 2019). Whether continuum models display the emergent properties of natural seismicity is then the key to bridging the gap between single-fault rupture studies and regional seismic hazard analysis.

Past studies have established that partial ruptures emerge above a certain length-scale threshold, particularly the ratio between fault width and characteristic nucleation size W/L_∞ (Lapusta et al., 2000). Recently, Cattania (2019) systematically explored the parameter space using 1-D fault simulations and

showed that the modeled frequency-magnitude distribution approaches unity as this ratio exceeds 10^2. Simulations of elongate, parallel planar faults showed that a larger W/L_∞ promotes fault interaction and synchronized ruptures (Barbot, 2021). However, there is a lack of statistics from the produced sequence arising from fault interactions, partly because 3-D simulations are increasingly expensive as W/L_∞ increases. It is still unclear if and under which conditions resolved 3-D continuum simulations can spontaneously generate power-law magnitude distributions or a realistic inter-event time distribution.

This study uses a three-dimensional quasi-dynamic physics-based model to simulate an interacting three-segment en echelon fault embedded in an elastic 3-D half-space. We investigate whether the nucleation length scale alters seismic sequences on individual faults and system-wide. We will show that the resulting sequences display a characteristic frequency-magnitude distribution and that the inter-event times also satisfy the proposed empirical inter-event time distribution seen in natural catalogs (Saichev & Sornette, 2007). Our parameter exploration produces a range of seismic behavior, from synchronized clusters at large critical slip distance D_c to clustered full and partial ruptures as D_c decreases. The paper first briefly discusses the methodology and model setup in section 2. Then we present results and offer comparisons to statistical models in section 3. Finally, in section 4, we discuss the broader context and present conclusions.

2 Methods

2.1 Model Descriptions

We simulate fault slip and stress transfer on three 2-D planar faults embedded in a 3-D half-space (Figure 1a). The rate-and-state friction law governs the fault friction. We use the regularized formulation presented by Ben-Zion and Rice (1997), Lapusta et al. (2000), and Rice and Ben-Zion (1996) to account for the singularity near-zero slip rates.

$$\mu = a \sinh^{-1} \left[\frac{V}{2V^*} \exp \left(\frac{\mu^* + b \ln\left(\frac{V^*\theta}{D_c}\right)}{a} \right) \right] \#(1)$$

Here, μ is the friction coefficient; V^* and μ^* are the reference slip rate and reference friction coefficient; a and b are constitutive parameters that scale the rate and state dependence of the coefficient of friction, respectively; D_c is the critical slip distance over which the state variable θ evolves. We use the Dieterich-Ruina aging law to describe the evolution of the state (Dieterich, 1978; Ruina, 1983):

$$\frac{\mathrm{d}}{dt} = 1 - \frac{V\theta}{D_c}.\#(2)$$

The equation of elastostatic equilibrium relates the stress state and friction to the slip rate on a point of a fault (Rice, 1993),

$$\tau_0 + \tau_e - \frac{G}{2c}V = \sigma\mu, \#(3)$$

where τ_0 is the plate loading shear stress; τ_e is the elastic shear stress from dislocation on any other part of the fault; σ is the normal stress; G/2c is the radiation damping term that bounds the slip rate from unrealistic values. Taking the time derivative of (3) and substitute friction μ with (2) and the time derivative of (1), we can obtain two coupled ordinary differential equations (ODEs) of $\dot{V}$ and $\dot{\theta}$ for each node (van den Ende et al., 2018). The slip-stress relations used to obtain τ_e are calculated using the rectangular finite dislocation solutions and accompanying module DC3D formulated by (Okada, 1992). The simulations are performed using the boundary element software QDYN (Luo et al., 2017). Galvez et al. (2019) implemented the hierarchical matrix (H-matrix) compression to the Greens function relating slip and stress tensors in QDYN (Bradley, 2014), thus replacing the fast Fourier transform method and allowing non-uniform meshes such as a bending fault or multiple disconnected faults.

In this study, we further improve QDYN's time-stepping efficiency by implementing the LSODA solver (Hindmarsh, 1983; Petzold, 1983). When integrating the rate-and-state ODEs during the interseismic period, the slip rate is of the order of 10^{-16} or smaller while θ is around 10^8. The system becomes stiff. Explicit solvers such as the Runge-Kutta methods require very small steps to be numerically stable (Erickson et al., 2008). This becomes a problem when we attempt to simulate multiple seismic cycles in a reasonable time. The LSODA solver monitors the stiffness of the system and automatically switches between Adams methods (predictor-corrector) in the non-stiff case and backward differentiation formula (BDF) methods (Gear methods) in the stiff case. The implementation is successful in that the iterations spent in interseismic time are largely reduced without sacrificing the resolution of each event. Using a Runge-Kutta solver of order 4 and 5, a full rupture takes approximately 9,000 iterations while interseismic periods take around 500,000 iterations. After switching solver, a full rupture on a fault section takes about 22,000 iterations, while an extended interseismic period takes around 37,000 iterations to complete.

2.2 Experiment Setup

To study the importance of fault interactions in a realistic yet simple geometry, we design a system of three en echelon right-lateral faults. Each fault has the same geometry and distribution of frictional properties (Figure 1). A fault measures 32 km by 24 km in size. A 3-km wide velocity-strengthening padding and 1-km transition belt surround the velocity-weakening patch (Figure 1a). The frictional behaviors are decided by a and b-values (Figure 1b). The seismogenic region is then ~26 km × 18 km. The segments are offset by 1 km and overlapped by 9 km. If the velocity-strengthening zone is excluded, the seismogenic regions overlap for 3 km. The overlap and offset are computed given the fault length based on scaling relations from field observations (de Joussineau & Aydin, 2009; Klinger, 2010). We use grid sizes of 143 m and 200 m. They are chosen to be

at least one third or smaller than the minimum length of an unstable slip L_b (Dieterich, 1992; Rubin & Ampuero, 2005), given by

$$L_b = \frac{GD_c}{b\sigma}.\#(4)$$

We do not enforce any additional heterogeneity on the fault surfaces. Studies have shown that even on a single fault, stress heterogeneity and complex ruptures can emerge without enforcing heterogeneity (Barbot, 2019; Cattania, 2019; Heimisson, 2020). In particular, the rupture mode starts to deviate from single-event cycles when the ratio of seismogenic width W and critical nucleation length L_∞ is large enough:

$$L_\infty = \frac{GD_c b}{(b-a)^2}, \#(5)$$

where G is the shear modulus; a, b, and D_c are rate-and-state friction parameters; σ is the effective normal stress (Rubin & Ampuero, 2005). Cattania (2019) found that for a 1-D fault, the minimum ratio to generate two and more events per cycle is ~10. We test the ratios from 10.82 to 32.47 by varying only D_c and keeping the profile of a, b, and σ fixed in all simulations. We also test the effect of loading rate on nucleation style using three different values: 5, 35, and 50 mm/year. All other parameters and initial conditions remain the same for all simulations (see Table S1).
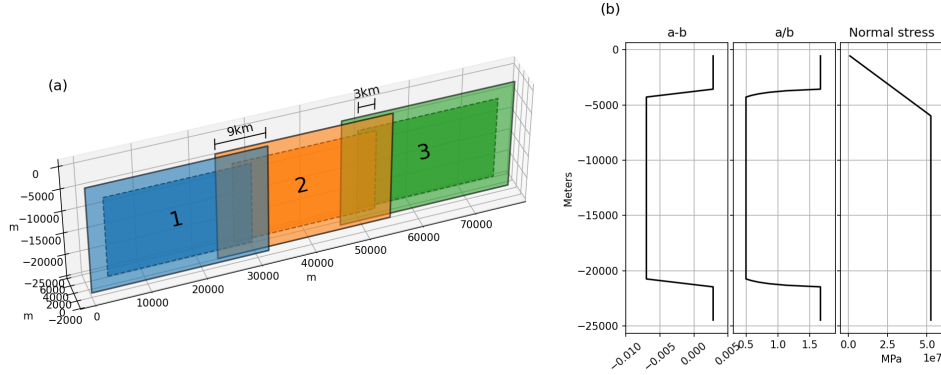

Figure . Model setup visualizations. (a) Model geometry and fault numbering. (b) The profiles of frictional parameters. Opaque patches at the center of the faults mark the velocity-weakening regions, corresponding to the profile where a-b = -0.007 and a/b = 0.5. There is a 1-km buffer zone between two frictional regimes. The normal stress linearly increases from 1 MPa at fault top to 52.5 MPa at 6 km and remains constant afterward.

We initiate all the simulations with the initial slip rates equal to 0.99, 1.01, and 1 time V_{PL} on faults 1, 2, and 3 respectively, and let initial state $\theta = D_c/V_{\mathrm{PL}}$, which is also the reference state. We run every simulation until there are more than 100 seismic events. Each simulation runs on a node of 24 cores and typically takes less than 360 hours to finish.

3 Results

3.1 Model Behavior and Sequence Statistics

We present eight simulations. For D_c equals 10 and 14 mm, we simulate three loading rates: 5, 35, and 50 mm/year. We run two additional simulations using larger D_c values of 20 mm and 30 mm and a slip rate of 50 mm/year. Visualizations of each sequence and the catalogs are presented in Figure S1 (see Supplementary Materials).

A typical seismic cycle from one full rupture on a fault to another consists of several partial ruptures and slow-slip events in between two mainshocks (Figure 2 and Movie S1). The slip velocity on the three faults distinguishes different slipping states. Blueish green represents areas close to the loading rate. Deep purple shows the locked areas. Warm colors indicate areas that is seismically slipping. In Figure 2a, fault 1 on the left has just entered the post-seismic locking stage as the slip rate in a seismogenic patch drops with time (Figure 2a–d), while faults 2 and 3 are further advanced in their seismic cycles. The slip rate starts to increase at the overlapped area of fault 3, and an event of M5.7 nucleates (Figure 2b). Slow-slip events also occur on the periphery of locked areas (Figure 2c). Partial ruptures continue to nucleate at the overlapping area and the outer corners, creating patches of "velocity" asperities and irregular seismicity. Finally, a full rupture on fault 3 (Figure 2j) resets the heterogeneous slip rate distribution and returns the slip rate distribution to a similar distribution to fault 1 in Figure 2a. In our model, partial ruptures act like foreshocks before a mainshock resets the slip rates and states back to a uniform distribution. In addition, partial ruptures cascade around the edge of seismogenic zones while full ruptures propagate the whole seismogenic zone and rupture the foreshock regions again.
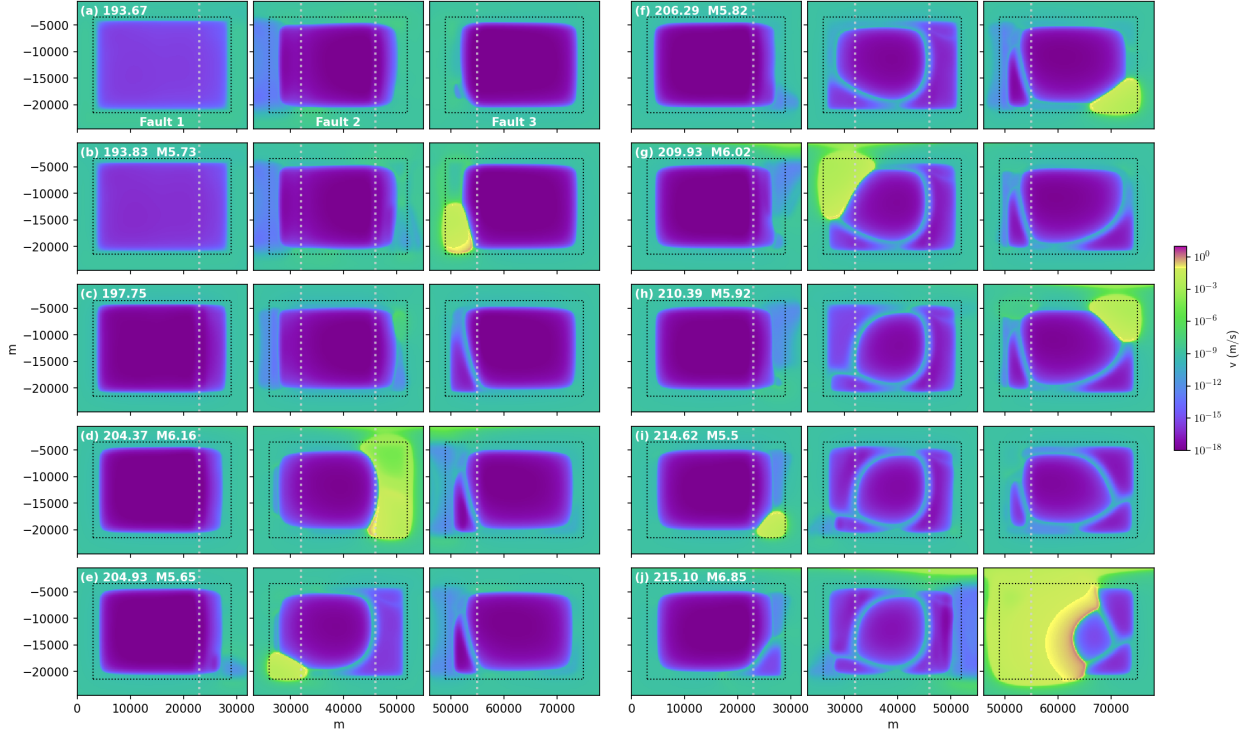
Figure . Snapshots of the slip rate field during a seismic cycle. Subplots a–j show 10 snapshots in subsequent time (years) and event magnitudes. Warm colors mark the seismically slipping patches with slip rates larger than 0.1 m/s. Black dashed lines outline the seismogenic velocity-weakening patches. Grey dashed lines mark the overlaps as seen from the side (Figure 1a). Snapshots are from the simulation with $W/L_\infty = 32.47$ and a loading rate of 50 mm/year.

In agreement with the 2-D single-fault case (Cattania, 2019), we find that simulations with a larger W/L_∞ ratio produce seismicity with frequency-magnitude distribution closer to what is observed in nature (Figure 3a). Note that we do have a significant portion of characteristic events. A ratio of 32.47 gives the partial ruptures a b-value of 0.5, while the b-value decreases to 0.3 when the ratio is 23.19. More partial ruptures also mean smaller magnitudes for characteristic events. On the other hand, loading rates have a very slight effect on the b-value in that the b-values seem to be larger when loading rates are higher, but the effect is negligible compared to the W/L_∞ ratio. We find that for our model setup, partial ruptures cease to emerge at $W/L_\infty = 10.82$ ($D_c = 30$ mm).

Our catalogs also reproduce the empirical inter-event time distribution and its coefficients proposed by Saichev and Sornette (2007) based on the Omori-Utsu law (Figure 3b). The two simulations with ratios equal to 10.82 and 16.24 deviate from the curve (black and grey circles respectively), suggesting that

8

characteristic events plus fault interaction alone do not create the inter-event time distribution (Figure S1). These simulations produce synchronized clusters shown as the bi-modal distribution of very short and very long inter-event time.

The six simulated sequences with ratios of 23.19 and 32.47 fit both a short-term Omori decay of t^{-p} and a long-term Poisson process that distributes exponentially. A dip exists at the simulated inter-event time distribution at the onset of exponential decay around 0.1 normalized time (Figure 3b), suggesting that our fault system only produces the two end-member distributions. The transition between the two is filled either by a weaker-coupled fault system or by other physical processes with a longer time scale of interaction.
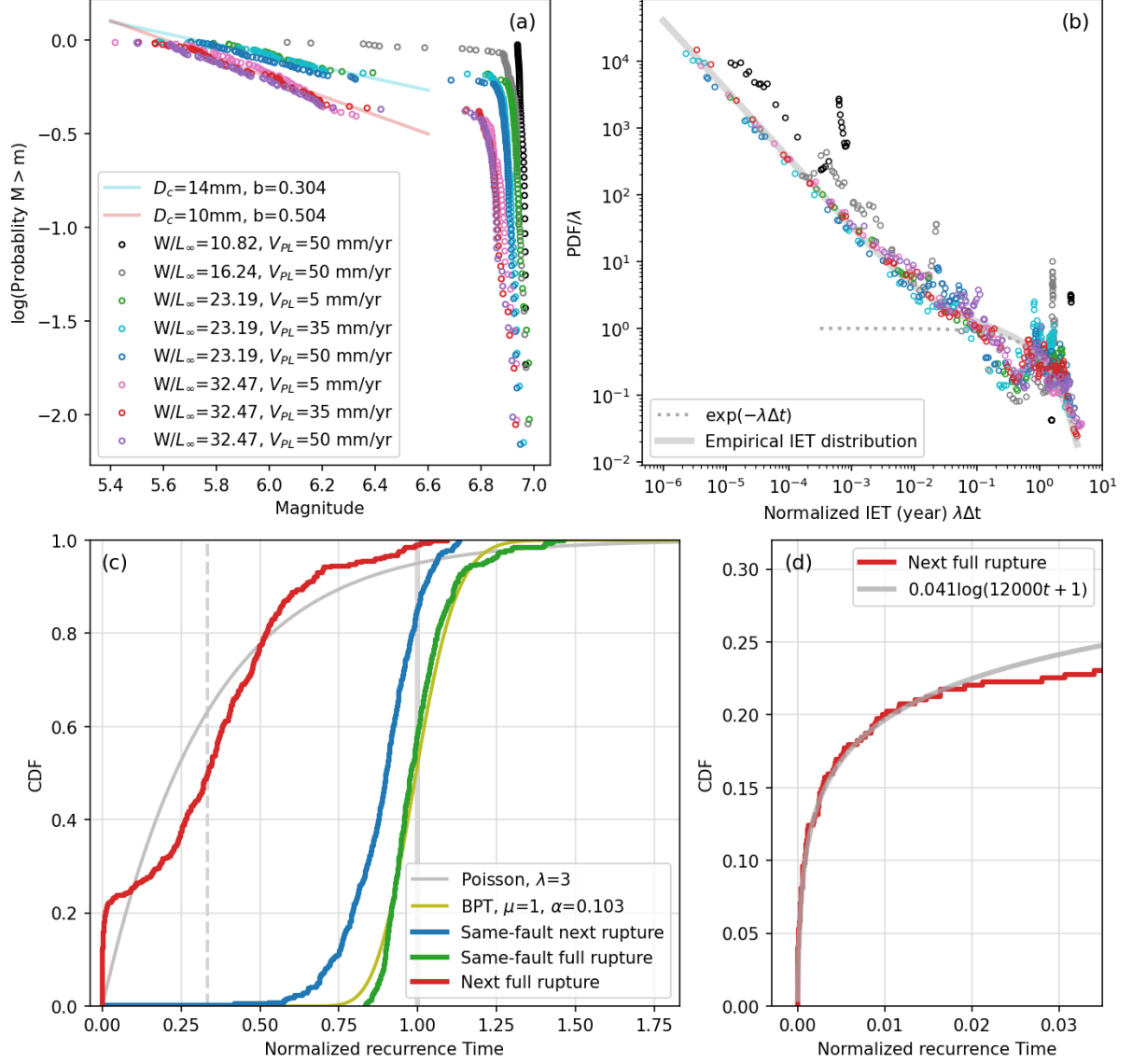
Figure . Statistics characters of simulated seismicity. (a) Frequency-magnitude
statistics of all eight simulations. (b) The normalized inter-event time of all
simulations against the empirical inter-event time distribution of Saichev and
Sornette (2007). We explore the influence of D_c and loading rate on the se-
quences produced. This shows that D_c, which scales L_∞, affects the ratio of
partial ruptures to full ruptures and the b-values. The inter-event time dis-
tribution fits the empirical distribution better when more partial ruptures are
present. (c) CDF of recurrence time normalized by the averaged single fault
return time. The green curve: CDF of the next full ruptures on the same fault.

The olive-color curve: BPT CDF with the aperiodicity taken from the sequence C_V. The blue curve: recurrence time to the next event, including partial events, on the same fault. The red curve: the CDF of the system-wide full rupture occurrence. We see a ~20% chance of another segment rupturing immediately after a full rupture and a drop of probability between 0.1 and 0.5 compared to a Poisson distribution. Grey vertical dashed and solid lines mark 1/3 and 1 normalized recurrence time. Magnifying the immediate recurrence time from 0 to 0.04 in (d), we observe an Omori-type rate decay that we manually fit with a log curve and a negative deviation after 0.02.

3.2 Recurrence Times

The spontaneous emergence of an inter-event time distribution very similar to the empirically observed ones gives us the confidence to examine the conditional probability of the next event after the occurrence of a full rupture 1) on a fault and 2) within the system. We summarize the recurrence times of the six sequences that have good fits to the empirical inter-event time distribution in Figure 3c–d. We analyze the cumulative density functions (CDFs) of the single-fault mainshock recurrence time (green), single-fault recurrence time including partial ruptures (blue), and system-wide mainshock recurrence time (red). Due to the different loading rates, the recurrence times are normalized by the averaged single-fault recurrence time of each sequence before combining.

Our models show that first, the mainshock recurrence times on a single fault remain quasi-periodic even if partial ruptures and fault interactions are present. The coefficient of variation (C_V), or the standard deviation over the mean, is 0.103. We compare the distribution with a Brownian passage time (BPT) distribution with its mean equal to 1 and aperiodicity equal to its C_V computed from the simulated sequence (Matthews et al., 2002). The theoretical (dark green) and simulated CDFs agree well, except that the simulated sequences have a longer tail. If we consider the recurrence from one mainshock to another shock on the same fault (blue curve in Figure 3c), thus including partial events, the distribution becomes left-skewed, confirming that the partial ruptures act like foreshocks. The onset time is around 0.5 recurrence time.

Finally, we calculate the system recurrence time, meaning the time between one mainshock and another mainshock within the system. The null hypothesis is a memoryless Poisson distribution of rate = 3 shown in grey in Figure 3c. The system CDF in red deviates from the Poisson CDF. About 22% of the mainshock pairs occur within 0.02 normalized return time, representing strong clustering in time. From 0.02 and beyond, the shape of the remaining CDF resembles the BPT distribution. The highest probability falls at around one third of the recurrence time (grey dashed line), but the spread is wider than single-fault BPT. Focusing on the first 0.04 normalized return time segment in Figure 3d, we see an Omori-type decay that we can manually fit with a log function up to around 0.2.

From this analysis, we derive that in our model setup, there is a one-fifth chance

of another mainshock on a nearby fault immediately following a mainshock. Beyond the first 2% of normalized fault return time, the next mainshock can occur at any time within the fault recurrence time.

4 Discussion and Conclusions

In this study, we demonstrate that a simple simulated fault system, which resembles natural fault geometry, can generate realistic earthquake statistics, including a realistic earthquake size distribution, clustering, and realistic inter-event times. These statistics are not prescribed in the model but emerge from first-order physical representation and interaction between faults. Because our models are well resolved in the continuum domain, it preserves rich and realistic slip behaviors independent of model meshing.

Our result shows that in 3-D, fault geometry plays an essential role in producing the power laws observed in regional seismicity. Our model produces frequency-magnitude distributions with characteristic, system-level earthquakes. A gap of 0.5 to 0.75 magnitude units separates full and partial ruptures. Below the gap, events have a power-law scaling with small b-values of 0.3 to 0.5 (Figure 3). This low b-value may be due to the limitation of the ratio of W/L_{∞} that we can reasonably simulate. It is likely that the b-value would approach unity as the ratio grows, as seen in the 1-D experiment and large regional catalogs like California (Cattania, 2019; Field et al., 2014). However, as noted first by Wiemer and Wyss (1997) for the Parkfield asperity, and later confirmed in other places (Tormann et al., 2015), when mapping b-values with high spatial resolution, the actual asperities that will rupture in mainshock are characterized by a b-value of 0.5 (Schorlemmer & Wiemer, 2005).

As for the long-standing debate in seismology about whether faults and fault systems show Gutenberg-Richter or characteristic earthquake distributions, our results suggest that not only individual faults but also fault systems can exhibit characteristic behavior. In our simulations, we see that events of all sizes can occur, with a power-law size distribution, but only up to a certain threshold of ~M6.3 (Figure 3a). Beyond that threshold, all ruptures will be run-away full ruptures of magnitude 6.5 to 6.9. This kind of behavior is observed for earthquakes in Parkfield, for example. Since 1857, there have been six earthquakes with a magnitude of about 6 (Toppozada et al., 2002), but no events with magnitudes between 5.2 and 5.9. Our identical, homogeneous faults seem to mimic a mature fault zone like the Parkfield section. A more continuous magnitude-frequency distribution instead emerges from complex geometries and fault heterogeneity.

Our models reproduce Gutenberg-Richter relation and realistic inter-event time distributions with a simple fault system geometry we choose to be consistent with geological evidence. Studies summarized observations over the shear zones of different scales and found the ratio between faults and their steps maintains a fixed ratio as faults link up and smooth out through earthquake cycles (de Joussineau & Aydin, 2007; Stirling et al., 1996). In this regard, we can see our modeled fault system as a segmented fault that consists of steps: an inherent

roughness. In fault rupture studies, a power-law-inducing roughness is implemented by the heterogeneous frictional property, approximated shear resistance, or non-planar mesh (Dieterich & Richards-Dinger, 2010; Fang & Dunham, 2013; Heimisson, 2020; Hillers et al., 2006). Nevertheless, we show that simple segments instead of fractal topography or D_c distribution are already enough for power-law statistics. Since the cracks grow and coalesce in a self-similar way into the crustal faults, we would see a similar stress interaction exist over a similar volume around the cracks, thus creating the self-similar power laws observed in both seismicity and our simulations from the scale of damage zones to fault zones.

Complex seismicity does not occur when we model a single fault segment even with the highest W/L_∞ value of 35.18 (Movie S2). In other words, the good fit with empirical distributions is a consequence of the interaction within the fault systems. To have spontaneous partial ruptures on a single fault, a simulation study on megathrusts shows that W/L_∞ needs to reach about 60 (Michel et al., 2017). Studies show that the aspect ratio also affects rupture behaviors. The length-to-width threshold for complex sequences needs to be larger than ~3.4 (Hirose & Hirahara, 2004). The same behavior is also present in dynamic simulations of self-arrest ruptures (Weng & Yang, 2017). Barbot (2021) shows that one can generate partial ruptures with a low W/L_∞ of 5.33 but this requires an elongated seismogenic zone of 75 km by 10 km or a ratio of 7.5. Our seismogenic zone is 26 km by 18 km or a ratio of 1.44 on a fault. Elongated fault geometry is motivated by very long, plate-boundary strike-slip faults. However, even these faults are also segmented by step-overs and kinks, as seen by both source inversions and paleoseismicity (Howarth et al., 2021; Klinger, 2010; Mildon et al., 2016).

Therefore, fault geometry likely plays a significant role in controlling the seismicity, probably more so than frictional heterogeneity. The evidence comes from 1) ease of generating partial ruptures on short faults and 2) the nucleating positions of seismic events (Figure 2 and Movie S1). Excluding the first event, all events nucleate exclusively on the corners and step-overs once the stress field evolves away from the initial condition. Stress perturbations also restrict the partial events within the overlapped area (Figure 2d). The same phenomenon not only exists in jagged crustal faults but also happens on the Main Himalayan Thrust, where the ramp concentrates partial ruptures in between through-going events that reach the surface (Dal Zilio et al., 2019; Mildon et al., 2019; Sathiakumar & Barbot, 2021).

In section 3.2, we have shown that our model generates a meaningful conditional expectation of the next full rupture in a minimalistic setup. However, we did not conduct a complete sensitivity study, and there remain several relevant parameters that may affect the modeled earthquake statistics, e.g., different segment loading rates, other complex geometries, different faulting types, heterogeneous friction properties, and more. When building a fault database for hazard models, the slip rates often have the largest range of uncertainty attached (e.g.,

Basili et al., 2013; Litchfield et al., 2014). From our results, individual fault recurrence time largely falls within 20% around the mean, and we observe a heightened chance of ruptures on nearby faults. However, it is not clear how much the statistics will change if the loading rates are slightly different on each fault. Through interaction, it is possible that the clustering would average out the slip rate difference, so that every fault gives the same apparent slip rate. Experiments with the loading rate sensitivity will also show how the conditional expectation of the next event changes from a single fault to faults within a system. Moreover, we could further verify the uncertainties of current seismic hazard models by systematically performing more simulations.

The modeling approach we present here could readily be adapted to more complex fault systems and consider observed fault geometries and slip rates. The advances in computational efficiency that we have included are essential to moving towards simulation-based PSHA with 3-D continuum models, which is a medium- to long-term goal of our study.

Acknowledgments

Open Research

The simulations are performed using QDYN software (Luo et al., 2017) hosted on https://github.com/ydluo/qdyn with the integration of H-matrix (Bradley, 2014) (https://github.com/ambrad/hmmvp) and DLSODA solver within ODEPACK, a project from Lawrence Livermore National Laboratory, USA (https://computing.llnl.gov/projects/odepack).

References

Bak, P., & Tang, C. (1989). Earthquakes as a Self-Organized Critical Phenomenon. *Journal of Geophysical Research*, *94*(89), 635–637.Barbot, S. (2019). Slow-slip, slow earthquakes, period-two cycles, full and partial ruptures, and deterministic chaos in a single asperity fault. *Tectonophysics*, *768*, 228171.Barbot, S. (2021). A Spectral Boundary-Integral Method for Quasi-Dynamic Ruptures of Multiple Parallel Faults. *Bulletin of the Seismological Society of America*, *111*(3), 1614–1630.Basili, R., Kastelic, V., Demircioglu, M. B., Garcia Moreno, D., Nemser, E. S., Petricca, P., et al. (2013). European Database of Seismogenic Faults (EDSF) [Data set]. Istituto Nazionale di Geofisica e Vulcanologia (INGV). https://doi.org/10.6092/INGV.IT-SHARE-EDSFBen-Zion, Y. (2008). Collective behavior of earthquakes and faults: Continuum-discrete transitions, progressive evolutionary changes, and different dynamic regimes. *Reviews of Geophysics* , *46*(4), RG4006.Ben-Zion, Y., & Rice, J. R. (1997). Dynamic simulations of slip on a smooth fault in an elastic solid. *Journal of Geophysical Re-*

search: Solid Earth, *102*(B8), 17771–17784.Beroza, G. C., & Ide, S. (2011). Slow Earthquakes and Nonvolcanic Tremor. https://doi.org/10.1146/annurev-earth-040809-152531Bradley, A. M. (2014). Software for Efficient Static Dislocation-Traction Calculations in Fault Simulators. *Seismological Research Letters*, *85*(6), 1358–1365.Cattania, C. (2019). Complex Earthquake Sequences On Simple Faults. *Geophysical Research Letters*, *46*(17–18), 10384–10393.Dal Zilio, L., van Dinther, Y., Gerya, T., & Avouac, J. P. (2019). Bimodal seismicity in the Himalaya controlled by fault friction and geometry. *Nature Communications*, *10*(1), 1–11.Dieterich, J. H. (1978). Time-Dependent Friction and the Mechanics of Stick-Slip. *Pageoph*, *116*, 790.Dieterich, J. H. (1992). Earthquake nucleation on faults with rate-and state-dependent strength. *Tectonophysics*, *211*(1–4), 115–134.Dieterich, J. H., & Richards-Dinger, K. B. (2010). Earthquake Recurrence in Simulated Fault Systems. *Pure and Applied Geophysics*, *167*(8–9), 1087–1104.van Dinther, Y., Künsch, H. R., & Fichtner, A. (2019). Ensemble data assimilation for earthquake sequences: probabilistic estimation and forecasting of fault stresses. *Geophysical Journal International*, *217*(3), 1453–1478.Dublanchet, P. (2020). Stress-dependent b value variations in a heterogeneous rate-and-state fault model. *Geophysical Research Letters*, *47*(13). https://doi.org/10.1029/2020gl087434van den Ende, M. P. A., Chen, J., Ampuero, J.-P., & Niemeijer, A. R. (2018). A comparison between rate-and-state friction and microphysical models, based on numerical simulations of fault slip. *Tectonophysics*, *733*(July 2017), 273–295.Erickson, B. A., Birnir, B., & Lavallée, D. (2008). A model for aperiodicity in earthquakes. *Nonlinear Processes in Geophysics*, *15*(1), 1–12.Erickson, B. A., Jiang, J., Barall, M., Lapusta, N., Dunham, E. M., Harris, R., et al. (2020). The Community Code Verification Exercise for Simulating Sequences of Earthquakes and Aseismic Slip (SEAS). *Seismological Research Letters*, *91*(2A), 874–890.Fang, Z., & Dunham, E. M. (2013). Additional shear resistance from fault roughness and stress levels on geometrically complex faults. *Journal of Geophysical Research, [Solid Earth]*, *118*(7), 3642–3654.Faulkner, D. R., Jackson, C. A. L., Lunn, R. J., Schlische, R. W., Shipton, Z. K., Wibberley, C. A. J., & Withjack, M. O. (2010). A review of recent developments concerning the structure, mechanics and fluid flow properties of fault zones. *Journal of Structural Geology*, *32*(11), 1557–1575.Field, E. H., Arrowsmith, R. J., Biasi, G. P., Bird, P., Dawson, T. E., Felzer, K. R., et al. (2014). Uniform California earthquake rupture forecast, version 3 (UCERF3)—The time-independent model. *Bulletin of the Seismological Society of America*, *104*(3), 1122–1180.Field, E. H., Milner, K. R., Hardebeck, J. L., Page, M. T., van der Elst, N. J., Jordan, T. H., et al. (2017). A Spatiotemporal Clustering Model for the Third Uniform California Earthquake Rupture Forecast (UCERF3-ETAS): Toward an Operational Earthquake Forecast. *Bulletin of the Seismological Society of America*, *107*(3). https://doi.org/10.1785/0120160173Galvez, P., Somerville, P., Petukhin, A., Ampuero, J.-P., & Peter, D. (2019). Earthquake Cycle Modelling of Multi-segmented Faults: Dynamic Rupture and Ground Motion Simulation of the 1992 Mw 7.3 Landers Earthquake. *Pure and Applied Geophysics*. https://doi.org/10.1007/s00024-019-02228-xGutenberg, B., & Richter, C. F. (1944). Frequency of earthquakes in California. *Bulletin of the Seismo-*

logical Society of America, *34*(4), 185–188.Heimisson, E. R. (2020). Crack to pulse transition and magnitude statistics during earthquake cycles on a self-similar rough fault. *Earth and Planetary Science Letters*, *537*, 116202.Hillers, G., Ben-zion, Y., & Mai, P. M. (2006). Seismicity on a fault controlled by rate- and state-dependent friction with spatial variations of the critical slip distance. *Journal of Geophysical Research*, *111*(B1), B01403.Hillers, G., Mai, P. M., Ben-Zion, Y., & Ampuero, J.-P. (2007). Statistical properties of seismicity of fault zones at different evolutionary stages. *Geophysical Journal International*, *169*(2), 515–533.Hindmarsh, A. C. (1983). ODEPACK, A Systematized Collection of ODE Solvers. *IMACS Transactions on Scientific Computation*, *1*, 55–64.Hirose, H., & Hirahara, K. (2004). A 3-D Quasi-static Model for a Variety of Slip Behaviors on a Subduction Fault. *Pure and Applied Geophysics*, *161*(11), 2417–2431.Howarth, J. D., Barth, N. C., Fitzsimons, S. J., Richards-Dinger, K., Clark, K. J., Biasi, G. P., et al. (2021). Spatiotemporal clustering of great earthquakes on a transform fault controlled by geometry. *Nature Geoscience*. https://doi.org/10.1038/s41561-021-00721-4Huang, J., & Turcotte, D. L. (1990). Evidence for chaotic fault interactions in the seismicity of the San Andreas fault and Nankai trough. *Nature*, *348*(6298), 234–236.Jiménez, A. (2013). Cellular automata to describe seismicity: A review. *Acta Geophysica*, *61*(6), 1325–1350.de Joussineau, G., & Aydin, A. (2007). The evolution of the damage zone with fault growth in sandstone and its multiscale characteristics. *Journal of Geophysical Research*, *112*(B12). https://doi.org/10.1029/2006jb004711de Joussineau, G., & Aydin, A. (2009). Segmentation along Strike-Slip Faults Revisited. *Pure and Applied Geophysics*, *166*(10), 1575–1594.Klinger, Y. (2010). Relation between continental strike-slip earthquake segmentation and thickness of the crust. *Journal of Geophysical Research*, *115*(B7), B07306.Lapusta, N., Rice, J. R., Ben-Zion, Y., & Zheng, G. (2000). Elastodynamic analysis for slow tectonic loading with spontaneous rupture episodes on faults with rate- and state-dependent friction. *Journal of Geophysical Research*, *105*(B10), 23765–23789.Larochelle, S., Lapusta, N., Ampuero, J., & Cappa, F. (2021). Constraining Fault Friction and Stability With Fluid-Injection Field Experiments. *Geophysical Research Letters*, *48*(10). https://doi.org/10.1029/2020GL091188Litchfield, N. J., Van Dissen, R., Sutherland, R., Barnes, P. M., Cox, S. C., Norris, R., et al. (2014). A model of active faulting in New Zealand. *New Zealand Journal of Geology and Geophysics*, *57*(1), 32–56.Luo, Y., Ampuero, J.-P., Galvez, P., van den Ende, M. P. A., & Idini, B. (2017). QDYN: a Quasi-DYNamic earthquake simulator (v1.1).Matthews, M. V., Ellsworth, W. L., & Reasenberg, P. A. (2002). A Brownian Model for Recurrent Earthquakes. *Bulletin of the Seismological Society of America*, *92*(6), 2233–2250.Michel, S., Avouac, J.-P., Lapusta, N., & Jiang, J. (2017). Pulse-like partial ruptures and high-frequency radiation at creeping-locked transition during megathrust earthquakes. *Geophysical Research Letters*, *44*(16), 8345–8351.Mildon, Z. K., Toda, S., Faure Walker, J. P., & Roberts, G. P. (2016). Evaluating models of Coulomb stress transfer: Is variable fault geometry important? *Geophysical Research Letters*, *43*(24), 12,407-12,414.Mildon, Z. K., Roberts, G. P., Faure Walker, J. P., & Toda, S. (2019). Coulomb pre-

stress and fault bends are ignored yet vital factors for earthquake triggering and hazard. *Nature Communications*, *10*(1), 2744.Noda, H., & Lapusta, N. (2013). Stable creeping fault segments can become destructive as a result of dynamic weakening. *Nature*, *493*(7433), 518–521.Ogata, Y. (1988). Statistical Models for Earthquake Occurrences and Residual Analysis for Point Processes. *Journal of the American Statistical Association*, *83*(401), 9–27.Okada, Y. (1992). Internal deformation due to shear and tensile faults in a half-space. *Bulletin of the Seismological Society of America*, *82*(2), 1018–1040.Omori, F. (1895). On the aftershocks of earthquakes. *Journal of the College of Science*, *7*, 111–120.Petzold, L. (1983). Automatic Selection of Methods for Solving Stiff and Nonstiff Systems of Ordinary Differential Equations. *SIAM Journal on Scientific and Statistical Computing*, *4*(1), 136–148.Rice, J. R., & Ben-Zion, Y. (1996). Slip complexity in earthquake fault models. *Proceedings of the National Academy of Sciences of the United States of America*, *93*(9), 3811–3818.Rice, James R. (1993). Spatio-temporal complexity of slip on a fault. *Journal of Geophysical Research*, *98*(B6), 9885.Richards-Dinger, K. B., & Dieterich, J. H. (2012). RSQSim Earthquake Simulator. *Seismological Research Letters*, *83*(6), 983–990.Rubin, A. M., & Ampuero, J.-P. (2005). Earthquake nucleation on (aging) rate and state faults. *Journal of Geophysical Research*, *110*(B11), 1–24.Ruina, A. (1983). Slip instability and state variable friction laws. *Journal of Geophysical Research, [Solid Earth]*, *88*(B12), 10359–10370.Saichev, A., & Sornette, D. (2007). Theory of earthquake recurrence times. *Journal of Geophysical Research*, *112*(B4). https://doi.org/10.1029/2006jb004536Sathiakumar, S., & Barbot, S. (2021). The stop-start control of seismicity by fault bends along the Main Himalayan Thrust. *Communications Earth & Environment*, *2*(1), 1–11.Schorlemmer, D., & Wiemer, S. (2005). Microseismicity data forecast rupture area. *Nature*, *434*(7037), 1086.Schorlemmer, D., Werner, M. J., Marzocchi, W., Jordan, T. H., Ogata, Y., Jackson, D. D., et al. (2018). The Collaboratory for the Study of Earthquake Predictability: Achievements and Priorities. *Seismological Research Letters*, *89*(4), 1305–1313.Stirling, M. W., Wesnousky, S. G., & Shimazaki, K. (1996). Fault trace complexity, cumulative slip, and the shape of the magnitude-frequency distribution for strike-slip faults: a global survey. *Geophysical Journal International*, *124*(3), 833–868.Taroni, M., Marzocchi, W., Schorlemmer, D., Werner, M. J., Wiemer, S., Zechar, J. D., et al. (2018). Prospective CSEP Evaluation of 1-Day, 3-Month, and 5-Yr Earthquake Forecasts for Italy. *Seismological Research Letters*, *89*(4), 1251–1261.Toppozada, T. R., Branum, D. M., Reichle, M. S., & Hallstrom, C. L. (2002). San Andreas Fault Zone, California: M 5.5 Earthquake History. *Bulletin of the Seismological Society of America*, *92*(7), 2555–2601.Tormann, T., Enescu, B., Woessner, J., & Wiemer, S. (2015). Randomness of megathrust earthquakes implied by rapid stress recovery after the Japan earthquake. *Nature Geoscience*, *8*(2), 152–158.Tullis, T. E., Richards-Dinger, K. B., Barall, M., Dieterich, J. H., Field, E. H., Heien, E. M., et al. (2012). Generic Earthquake Simulator. *Seismological Research Letters*, *83*(6), 959–963.Utsu, T. (1961). A statistical study on the occurrence of aftershocks. *The Geophysical Magazine*, *30*, 521–605.Weng, H., & Ampuero, J.-P. (2019). The dynamics of elongated earthquake ruptures.

Journal of Geophysical Research, [Solid Earth], *124*(8), 8584–8610.Weng, H., & Yang, H. (2017). Seismogenic width controls aspect ratios of earthquake ruptures. *Geophysical Research Letters*, *44*(6), 2725–2732.Wiemer, S., & Wyss, M. (1997). Mapping the frequency-magnitude distribution in asperities: An improved technique to calculate recurrence times? *Journal of Geophysical Research*, *102*(B7), 15115–15128.